Identification and Distribution of Vanadinite (Pb-5(V5+O4)(3)Cl in Lead Pipe Corrosion By-Products

ARTICLE *in* ENVIRONMENTAL SCIENCE AND TECHNOLOGY · JULY 2009

Impact Factor: 5.33 · DOI: 10.1021/es900501t · Source: PubMed

3 AUTHORS, INCLUDING:

Kirk G Scheckel
United States Environmental Protection A…
147 PUBLICATIONS **3,880** CITATIONS
SEE PROFILE

Michael R Schock
United States Environmental Protection A…
93 PUBLICATIONS **1,270** CITATIONS
SEE PROFILE

Identification and Distribution of Vanadinite ($Pb_5(V^{5+}O_4)_3Cl$) in Lead Pipe Corrosion By-Products

TAMMIE L. GERKE,[†] KIRK G. SCHECKEL,[‡] AND MICHAEL R. SCHOCK*,[‡]

Department of Geology, University of Cincinnati, Cincinnati, Ohio 45221-0013, and U.S. Environmental Protection Agency, National Risk Management Research Laboratory, 26 West Martin Luther King Drive, Cincinnati, Ohio 45268

Received February 16, 2009. Revised manuscript received April 20, 2009. Accepted April 28, 2009.

This study presents the first detailed look at vanadium (V) speciation in drinking water pipe corrosion scales. A pool of 34 scale layers from 15 lead or lead-lined pipes representing eight different municipal drinking water distribution systems in the Northeastern and Midwestern portions of the United States were examined. Diverse synchrotron-based techniques, including bulk XANES (X-ray absorption near edge spectroscopy), μ-XANES, μ-XRD (X-ray diffraction), and μ-XRF (X-ray fluorescence) mapping were employed along with traditional powder XRD, SEM-EDXA (scanning electron microscopy−energy dispersive X-ray analysis), and ICP-OES (inductively coupled plasma−optical emission spectrometry) to evaluate vanadium speciation and distribution in these deposits. Vanadinite ($Pb_5(VO_4)_3Cl$) was positively identified, and occurred most frequently in the surface layers. Low V_{tot} in these waters is likely the limiting factor in the abundance of vanadinite in the pipe scales, along with the existence of divalent lead. The occurrence of V in these samples as a discrete mineral is important because it is formed in the presence of very low concentrations of V in the finished water, it provides a mechanism to concentrate $\mu g \cdot L^{-1}$ amounts of V from the water to near-percent levels in the pipe scales, and the robustness of V accumulation and release in response to water chemistry changes is likely different than it would be with a sorption accumulation mechanism. Extrapolation from limited existing water chemistry data in this study provides an estimate of ΔG_f° for vanadinite as approximately −3443 $kJ \cdot mol^{-1}$, or less, leading to a log K_{s0} value of approximately −86 for the reaction

$$Pb_5(VO_4)_3Cl_{(s)} \rightleftarrows \{Pb^{2+}\}^5 + \{VO_4^{3-}\}^3 + \{Cl^-\},$$

in which {}denotes activity.

Introduction

Vanadium can be either beneficial or toxic to humans, depending on its oxidation state and concentration and its toxicity increases with increasing oxidation state (*1–4*). In natural and drinking waters, vanadium dominantly exists in either the +4 or +5 oxidation state as the aquatic species vanadyl (VO_3^{2-}) or vanadate (VO_4^{3-}), respectively (*5–8*). V^{IV} would be the most stable in reducing environments and V^V (vanadate) is expected to be prevalent in systems consistently exposed to atmospheric oxygen (*5*), and hence, would be expected in disinfected or preoxidized drinking waters. Vanadate behaves similarly to orthophosphate, and will form ligand exchange surfaces with hydrous phases such as iron oxyhydroxides (*8, 9*). V^{III}, however, would rarely be found in potable waters because of being readily oxidized by air or dissolved oxygen.

Researchers have modeled the V^{3+} metal ion, forming several hydroxide complexes including VOH^{2+}, $V(OH)_2^+$, and $V(OH)_3^\circ$. Modeling of aqueous vanadyl speciation shows greater variation. Wehrli and Stumm (*8*) assumed the aqueous vanadyl species included the oxocations VO^{2+} and $VO(OH)^+$; the neutral species $VO(OH)_2^\circ$; the oxoanion $VO(OH)_3^-$; and the polymeric oxocation $(VOOH)_2^{2+}$. However, Langmuir (*10*) only included VO^{2+} and $VO(OH)^+$ as vanadyl species (*10, 11*). Wanty and Goldhaber (*12*) have presented perhaps the most extensive critically evaluated compilation of thermochemical data for aqueous V species, including several vanadyl complexes with carbonate, oxalate, acetate, sulfate, fluoride, and chloride. In spite of the differences in the details of the aqueous model for V^{IV}, the general predominance trends predicted by Wehrli and Stumm (*8*), Wanty and Goldhaber (*12*), and Langmuir (*10*) are similar (Supporting Information Figure SI1).

Ingestion of vanadium from drinking water has recently been considered a potentially serious threat to human health because of the growing body of evidence regarding the human toxicity of vanadium (*1–4*). The concentrations of vanadium in United States drinking waters have not been comprehensively surveyed, because without a regulatory driving force, vanadium is rarely monitored by public or private water utilities. Regardless, in 2007 the California Office of Environmental Health Hazard Assessment set a notification level of 15 μg/L for vanadium in drinking water (*13*), and it has been listed by the U.S. Environmental Protection Agency in the draft Drinking Water Contaminant Candidate List 3 (*14*). Recently, the accumulation of vanadium up to as much as 2% by weight, has been reported for corrosion deposits in lead drinking water pipes from numerous United States public drinking water systems (*15*). Thus, a potential reservoir for human exposure already exists if vanadium were to be mobilized by changes in drinking water characteristics resulting from source or treatment changes.

This study presents the first detailed look at vanadium speciation and distribution in drinking water pipe corrosion scales. Diverse synchrotron-based techniques, including bulk XANES (X-ray absorption near edge spectroscopy), μ-XANES, μ-XRD (X-ray diffraction), and μ-XRF (X-ray fluorescence) mapping along with traditional powder XRD, SEM-EDXA (scanning electron microscopy−energy dispersive X-ray analysis) and ICP-OES (inductively coupled plasma−optical emission spectrometry) were used in this study to evaluate vanadium speciation and distribution in these deposits.

Fifteen lead pipe samples from eight different municipal drinking water distribution systems in the Northeastern and Midwestern regions of the United States representing a wide range of water chemistries and treatments were selected for this study, and were chosen on the expectation of giving the highest potential for differences in V speciation (Table 1). Six pipe samples received treated water from surface sources and two from groundwater sources. Corrosion control treatment strategies listed in Table 1 reflects current utility operations, not historical treatment strategies. Therefore,

* Corresponding author phone: 513-487-7412; fax: 513-569-7172; e-mail: Schock.Michael@epa.gov.
[†] University of Cincinnati.
[‡] National Risk Management Research Laboratory.

10.1021/es900501t CCC: $40.75

Published on Web 05/12/2009

TABLE 1. Summary of Samples Analyzed in This Study, with Type of Source Water, Current Applied Corrosion Treatment, V and Pb Concentrations, Types of Analyses Conducted on Each

								XANES		μ-XRD	μ-XANES	
sample ID	source water	corrosion treatment	layer	V ppm	Pb %	macro XRD	ICP		V*	V*		V*
A1	S	OP	L1	2760	69.0	X	X	X	X			
			L2	–	–	X						
A2	S	OP	L1	1900	75.2	X	X	X	X			
			L2	1200	74.8	X	X	X	?			
A3	S	OP	L1	6540	67.6	X	X	X	X			
			L2	–	–	X						
			L3	1380	86.0	X	X	X	X			
A4	S	OP	L1	4310	81.4	X	X	X	X			
			L2	2730	82.2	X	X	X	X			
			L3	2710	79.6	X	X	X	X			
			L4	1560	84.4	X	X	X	X			
A5	S	OP	L1	6330	40.6	X	X	X	X			
			L2	–	–	X		X	X			
			L3	3600	71.6	X	X	X	X			
A6	S	OP	L1	–	–	X				X	X	X
			L2	8500	52.2	X	X				X	
			L3	2750	62.9	X	X				X	
A7	S	OP	L1	5480	40.6	X	X			X	X	X
			L2	2650	50.2	X	X				X	
			L3	716	67.9	X	X				X	
B1	S	CP	whole	<40	72.2	X	X	X				
C1	S	CP	L1	323	47.2	X	X					
			L2	23	84.7	X	X	X				
			L3	–	–	X						
D1	GW	CP	L1	2630	41.7	X	X	X	X			
E1	S	BP	L1	–	–	X						
			L2	330	70.3	X	X	X	?			
			L3	–	–	X						
F1	S	BP	L1	1900	43.8	X	X	X	?			
G1	S	CP+PP	L1	2200	73.7	X	X	X	X			
H1	S	CP	L1	2200	42.6	X	X	X	X			
I1	GW	CP	L1	237	86.0	X	X			X	X	X
			L2	779	70.0	X	X				X	X
			L3	676	60.6	X	X				X	

S, surface water; GW, ground water; V* = *X* = vanadinite identified (? = probable but not definitive); CP, carbonate passivation (which may include PbO_2 formation); OP, orthophosphate addition; BP, blended phosphate addition; PP, polyphosphate scale control.

direct V speciation consequences of historical treatment changes cannot readily be determined.

Experimental Section

Lead pipes were bisected longitudinally using a variable speed band-saw with a carbon steel blade, and deposit samples were collected from one-half. The other was stored for archival reference. Sections cut from these reference segments served as the source for the micro synchrotron analyses. Scale subsamples of approximately 0.2 to 1 g were harvested with stainless steel spatulas and other precise tools from layers and features based on apparent texture and color differences. Materials were ground by hand with an agate mortar and pestle, until they passed through a 200 (75 μm) mesh stainless steel sieve.

Powder XRD (Scintag XDS-2000) with Cu Kα radiation, with a curved crystal monochromator and Peltier detector provided an initial analysis of bulk crystalline phases for all samples. Scale material from 27 layer samples having sufficient volume, were analyzed for a minimum of 40 elements by ICP-OES(*16*) at the U.S. Geological Survey in Denver. Only vanadium and lead concentrations are reported here (Table 1). Samples from 19 layers were analyzed by XANES. For micro analyses to determine mineral position in situ, three samples were specially prepared and slide mounted for μ-XRF, μ-XANES, and μ-XRD. The synchrotron analyses were performed at the XOR/PNC beamlines (Sector 20-BM and 20-ID) at the Advanced Photon Source (APS, Argonne National Lab, Argonne, IL). Bulk XANES analyses were performed at the XOR/PNC 20-BM beamline, while μ-XRF, μ-XANES, and μ-XRD analyses were done at the XOR/PNC 20-ID beamline. The monochromatic beam energy was set at 13.1 KeV for μ-XRF using a Si (111) channel-cut monochromator and the beam was focused to approximately 15 × 15 μm using rhodium-coated Kirkpatrick-Baez focusing optics. SEM-EDXA (JEOL 5800) identified morphology and elemental distribution for the in situ samples. Additional and detailed sample preparation and analytical techniques are in the SI.

Results and Discussion

Schock et al.(*15*) first reported vanadium concentrations for outer scale layers from a set of lead pipe scales from 26 municipal water systems in the United States that ranged from 13 to 22 000 ppm (n = 54 layers) with an average of approximately 2500 ppm. From this set, we selected 15 lead pipe samples from eight representative municipal water systems accounting for 34 individual layers of which 27 layers had significant material for ICP-OES and other elemental analyses (Table 1). The discovery of such high concentrations of vanadium suggested three important questions: (1) Can the speciation of vanadium in lead pipe corrosion byproduct be determined and predicted? (2) How vulnerable is the

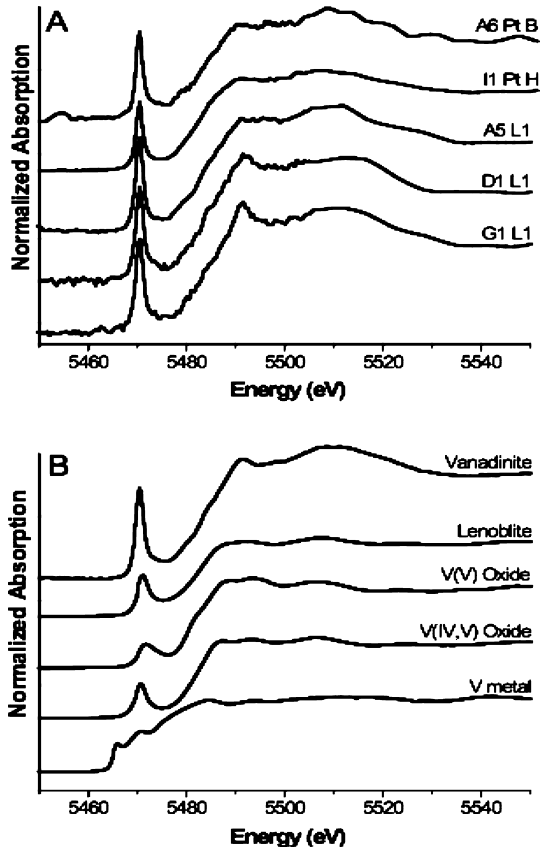

FIGURE 1. (a) Representative bulk XANES spectra for three samples and two representative μ-XANES spectra. Sample identifications correspond to Table 1; (b) bulk XANES spectra for vanadium standards.

vanadium in the pipe scales to be mobilized by hydraulic or water chemistry fluctuations? (3) What is the source of the vanadium?

Powder XRD analysis of all 34 layers was conducted (SI Table SI1). The primary crystalline lead phases in the samples varied with water chemistry and are consistent with lead corrosion theory (*17–19*). No unambiguously identifiable vanadium minerals were revealed by powder XRD. Discrete vanadium solid phases could be undetectable by powder XRD because they were either amorphous or a crystalline phase in low concentration. Therefore, a more robust analytical technique was needed to overcome the shortcomings of powder XRD. XANES allows for examination of amorphous and crystalline materials present in very low concentrations and has spectral features unique to the oxidation state and speciation of an element of interest.

Bulk XANES. XANES spectra were obtained for powdered scale layers which ranged in vanadium concentrations from 23 to 6540 ppm (Table 1). Fourteen XANES spectra have very distinct pre-edge vanadium peaks at 5469.5 eV. Three representative XANES spectra (A5 L1, D1 L1, and G1 L1) are presented in Figure 1a, and selected vanadium standards in Figure 1b. Nriagu has noted at least 80 known minerals that contain vanadium and categorized them into four main groups defined by depositional environments, oxidation states, and crystallography (*20*). However, the list of potential vanadium-rich phases that could be represented by these spectra can be reduced by considering the exposure of the pipes to an oxidizing environment, where the dominant aqueous V form would be the vanadate species. Vanadinite has a very distinct XANES spectrum with a dominant pre-edge derivative peak position at 5469.5 eV, a main edge peak position of about 5482 eV(*21, 22*), and a normalized pre-edge peak intensity of approximately 1(*21*). Wong et al.(*22*) and Chaurand et al.(*21*) developed very robust methods for the identification of V reference compounds based on the above characteristics as well as the area under the curve, centroid peak positions, and derivative peak positions of the main edge. Bulk vanadium XANES spectra collected in this study are identified as vanadinite ($Pb_5(VO_4)_3Cl$) based on the normalized pre-edge peak positions ranging from 5469.46 to 5469.5 eV, pre-edge intensities ranging from 0.989 to 1.048, and absolute derivative peak positions of the main edge from 16.44 to 16.52 eV (Table 2). These values are precisely in the ranges determined by Wong et al.(*22*) and Chaurand et al.(*21*) for vanadinite. Vanadinite has been found in natural environments as a secondary mineral with lead-bearing deposits, commonly associated with phases such as chloropyromorphite ($Pb_5(PO_4)_3Cl$) (*23*), cerussite, anglesite, calcite, and iron oxides (*24*).

Micro Synchrotron Analyses: μ-XRF mapping, μ-XRD, or μ-XANES. One representative lead pipe sample from two distribution systems (A6 and I1; Table 1) were cross-sectioned and mounted to allow analysis of their in situ corrosion byproduct using μ-XRF, μ-XRD, and μ-XANES (Figure 2a and b, SI Figure SI2, Figure 1a) in an attempt to identify vanadium-rich phases and their location within the corrosion byproduct deposit. An additional sample was analyzed (A7; Table 1) using μ-XANES (results not presented). Mapping of A6 and I1 by μ-XRF found regions of discrete high vanadium concentration which appeared to be mainly in the outermost portions of the corrosion byproduct (Figure 2a and b). These regions were additionally analyzed by either μ-XRD, μ-XANES, or both.

Consistent with the case of the bulk samples, if vanadinite is present it appears to be either quasicrystalline or present in such low concentrations that even with μ-XRD analysis the mineral is difficult to detect (SI Figure SI2). μ-XANES spectra were collected in other regions of elevated vanadium concentrations in samples A6 and I1 (Figure 2a and b) to determine if vanadinite could be positively located and identified within the scale. The μ-XANES spectra were very similar to the bulk XANES spectra (Figure 1a) with distinct normalized pre-edge peak positions (5469.46−5469.5 eV) and intensities (0.928−1.046) as well as absolute derivative peak positions of the main edge (16.44−16.52 eV) which support identification of the vanadium phase as vanadinite ($Pb_5(VO_4)_3Cl$) (Table 2) in these samples.

To further substantiate the identification of vanadinite in the bulk and micro analyzed samples, principal component analysis (PCA) and linear combination fitting (LCF) was conducted on the XANES spectra presented in Figure 1. SI Table SI2 demonstrates that vanadinite accounts for approximately 90−98% of the vanadium present in these samples, with the remaining amount identified as V(V) oxide. The bulk samples in Figure 1 noted lower vanadinite concentrations (89.8−92.6%) in comparison to 95.6−98.1% for the micro-XANES samples, highlighting an advantage of utilizing microfocused synchrotron techniques. The presence of V(V) oxide in the samples could suggest either that vanadate oxide is forming, or that vanadate ions are adsorbing to available Pb or other mineral surfaces within the pipe scale material. Notably, the two highest V(V) oxide cases correspond to pipe scales where 15−25% of the scale by weight was comprised of Fe, Mn, and Al-containing solids. V(V) oxide formation could also be a precursor step in the formation of vanadinite, analogous to the mechanism demonstrated for the formation of pyromorphite ($Pb_5(PO_4)_3Cl$) when phosphate ions were allowed to react with Pb(II) minerals (*25–28*).

SEM−EDXA. Additionally to examine the morphology of the vanadinite in the lead pipe scale materials surface regions were analyzed by SEM−EDXA for lead, vanadium, and chlorine. Crystals consisting of only these elements were acicular and fibrous (SI Figure SI3), which is one of the known

TABLE 2. Detailed XANES Analysis for Intensity and Position of Pre-Edge Peak and Derivative Main Edge Peak Position. Absolute and Main Edge Positions Are Presented Relative to Binding Energy of Elemental V (5465 eV)

	sample identification	normalized intensity	absolute position (eV)	main edge $E_{1/2}$ (eV)
bulk samples	A5 L1	0.996	4.50	16.50
	D1 L1	1.011	4.46	16.44
	G1 L1	0.998	4.47	16.47
	range of all bulk	0.989−1.048	4.46−4.50	16.44−16.50
micro samples	A6 PtB (Figure *2*a)	1.010	4.47	16.49
	I1 PtH (Figure *2*b)	0.928	4.49	16.44
	range of all micro	0.928−1.046	4.46−4.50	16.44−16.52
references	vanadinite[c]	0.996	4.50	16.49
	vanadinite[a,c]	0.920	4.60	16.10
	vanadinite[a,d]	1.160	4.40	16.30
	vanadinite[b,d]	1.060	4.50	~18.0
	lenoblite[c] ($V^{4+}{}_2O_4 \cdot 2(H_2O)$)	0.398	5.20	17.05
	V(V) oxide[c]	0.320	5.62	15.30
	V(IV,V) oxide[c]	0.381	4.71	14.71
	V metal[c]	0.281	0.98	8.80
	coulsonite[a,c] ($FeV^{3+}{}_2O_4$)	0.060	3.70	12.90
	$V^{4+}{}_2O_4$[a,d]	0.310	4.40	13.12
	pascoite[a,c] ($Ca_3V^{5+}{}_{10}O_{28} \cdot 17(H_2O)$)	0.480	5.30	15.40
	$Na_3V^{5+}O_4$[a,d]	1.150	4.80	15.00
	$NH_4V^{5+}O_3$[b,d]	0.910	4.80	17.20
	$CrV^{5+}O_4$[b,d]	0.820	4.80	17.60

[a] From ref *20*. [b] From ref *21*. [c] Si(111) mono. [d] Si(220) mono.

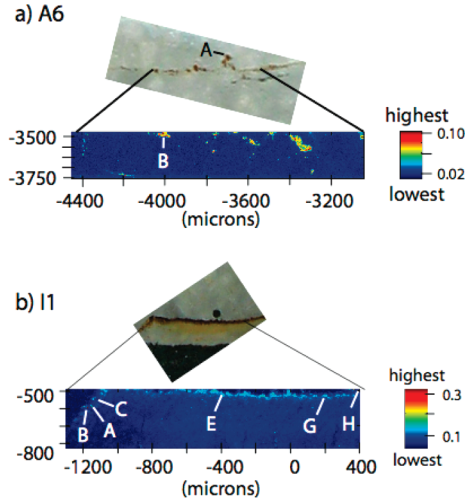

FIGURE 2. Thin section image and μ-XRF map of vanadium concentrations for the selected region (indicated by black lines) for samples (a) A6 and (b) I1. The lettered locations in the μ-XRF maps indicates the location of the representative μ-XANES spectra in Figure 1a.

morphologies of vanadinite. Thus, SEM−EDXA may be a viable identification tool for vanadinite in lead corrosion scales.

Overall, vanadinite most frequently was present in the surface (water contact) layer of the scales regardless of water system. The system studied where vanadinite was also present above 1000 $mg \cdot kg^{-1}$ levels in lower scale layers represented a unique situation in which a water system with historically high Pb corrosion formed extensive PbO_2 deposits during approximately 6−7 years of chlorine residual in excess of 3 $mg \cdot L^{-1}$ (*29, 30*). As a consequence of a treatment change to less-oxidizing chloramination, PbO_2 rapidly dissolved, with subsequent growth of replacement Pb(II) carbonates, hydroxycarbonates, and oxides on the surface and within the scale structure. Orthophosphate dosing started in the summer of 2004, causing additional transformation of the divalent lead hydroxycarbonates and oxides to various divalent lead orthophosphate compounds on and within the scale. Thus, an environment of high concentrations of Pb^{2+} species within the scale and at the surface existed that provided an exceptionally favorable opportunity for reaction with vanadate ions to form vanadinite. Based on tabulated equilibrium constant and Gibbs free energy data for the vanadate ion and PbO_2, redox and reductive dissolution reactions of vanadate ion with PbO_2 should not occur. Thus, vanadium accumulation in lead pipe scales as a defined solid phase would require water chemistry conditions that are in equilibrium with divalent lead solids (such as cerussite, hydrocerussite, or pyromorphite family phases), or would occur under redox conditions that favor the breakdown of PbO_2 and the release of Pb^{2+} ion.

Vanadinite and Chloropyromorphite Stability Diagrams. The stability and formation of vanadinite has been of considerable interest to geochemists. An extensive literature search did not uncover solubility data or Gibbs free energy data for vanadinite, with which phase relationships for drinking water conditions could be calculated. However, this study provides an opportunity to develop an initial estimation of the empirical solubility constant and a derived Gibbs free energy of formation value for vanadinite. Directly obtaining drinking water samples from premise plumbing that can be considered to be in actual equilibrium with vanadinite in the pipe scales is nearly impossible. Such samples would allow a straightforward calculation of the observed ion activity product (IAP) using any of several geochemical speciation computer models. However, a similar indirect strategy to that devised for some natural minerals by Garrels (*31*) can be used to derive an approximate upper limit of the solubility constant for vanadinite. Careful assumptions about the vanadium and lead levels commonly occurring within the pipes, and the range of key water quality parameters, can enable an approximate upper limit to the solubility constant for vanadinite to be derived. Linear combination fitting (SI Table SI2) further supports the assumption that vanadinite is essentially the controlling phase for V(V) in the scales.

Finished water chemistry information was obtained from one of the water utilities having substantial vanadinite in the

pipe scale, and currently using disinfection with chloramine and corrosion control with orthophosphate. The data (SI Table SI3) indicates that chloride varies seasonally from about 16 to 89 mg/L, and there are minor fluctuations in other water quality parameters such as pH, alkalinity, and orthophosphate concentration and average 7.6, 74 (as $CaCO_3$), and 2.3 mg/L (as PO_4), respectively. Vanadium levels have been observed to be below 0.0016 mg/L, with an average of 0.0009 mg/L.

Estimating the lead concentration is more complex. From practical utility sampling experience under the Lead and Copper Rule and plumbosolvency knowledge (*19, 32*), the lead concentrations upon prolonged stagnation in lead service lines can be assumed to be somewhat higher than those observed in first draw 1 L samples. For this system, which currently reports a 90th percentile level of 0.011 mg/L, the maximum soluble lead levels in the lead pipes are estimated to range from about 0.01 to 0.02 mg/L. However, during normal daily water use, the lead levels will often be considerably lower than that, as water is flushed through to varying extents. For a chloraminated water system, the Eh is estimated at being approximately 0.7 V, primarily based on observations of ORP vs dosage experiments by two research groups (*33, 34*). At this Eh, the stable valence states for lead and vanadium would be +2 and +5, respectively.

Using the general background water chemistry, assumptions about the limits of the highly varying water matrix constituents (which would affect ionic strength and particularly lead speciation), and presumed lead concentrations of 0.007, 0.01, and 0.015 mg/L, a range of log K_{s0} and ΔG_f° values for presumed equilibrium with vanadinite can be calculated (SI Table SI4). The computer program Geochemist's Workbench (Release 7, Rockware Inc., Golden, CO) was used to perform the speciation and IAP calculations (*35*), using the "thermo.dat" database furnished for vanadium and major constituent reactions, and log *K* values for aqueous Pb species from NIST (*36*) and Schock et al. (*19*) (SI Table SI5). Temperature was assumed to be 25 °C, because reliable temperature adjustments for equilibrium constants do not exist for most critical Pb and V species. Sodium was used to balance charge, as it would have minimal impact on the actual fraction of the metals complexed. For the reaction

$$Pb_5(VO_4)_3Cl_{(s)} \rightleftarrows \{Pb^{2+}\}^5 + \{VO_4^{3-}\}^3 + \{Cl^-\} \qquad (1.1)$$

the average observed IAP for different ranges of chloride and lead concentrations was $10^{-86.1}$, from which ΔG_f° for vanadinite can be calculated as approximately −3443 kJ·mol^{-1} using standard relationships. These likely represent an upper bound to the solubility of vanadinite, as during normal water usage and flow patterns in the premises, as well as with typical treatment and seasonal water variability, lead and vanadium concentrations are probably usually lower than the assumptions here. Using this data, the new Eh−pH relationships for lead minerals are shown in Figure 3a and b for one set of water chemistry conditions applicable to many surface water systems.

Two particularly intriguing questions that arise from this work are (1) whether lead pipes represent a unique medium for the accumulation of vanadium because of the ability of Pb to form the specific mineral vanadinite and (2) whether or not the presence of vanadium in drinking water would accumulate in scales, sediments in pipes, or storage tanks of different materials or sediment deposits (such as ferric or manganic oxyhydroxides) via a different mechanism. The sensitivity to water chemistry or hydraulic fluctuations would likely differ if the accumulation mechanism varied. For example, a recent study showed that vanadium sorbs readily on synthetic ferrihydrite (*37*), which is not dissimilar to many scales on unlined cast iron pipes. Given that vanadinite is

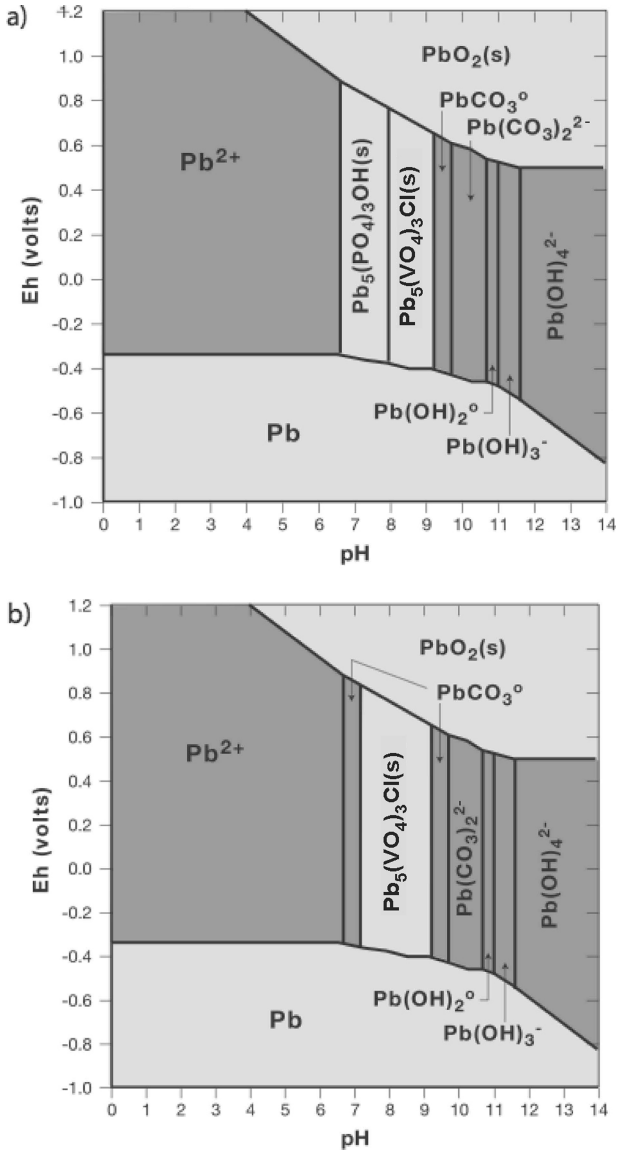

FIGURE 3. (a) Vanadinite and hydroxypyromorphite stability with estimated log K_{sp} value from this work. Conditions: Pb activity = 0.01 mg/L, DIC = 18 mg C/L, chloride 16 mg/L and orthophosphate = 2.3 mg/L as PO_4, ionic strength = 0, 25 °C and (b) Vanadinite and chloropyromorphite stability with estimated log K_{sp} value from this work. Conditions: Pb activity = 0.01 mg/L, DIC = 18 mg C/L, chloride 16 mg/L, ionic strength = 0, 25 °C.

often found in association with iron-ore mineral phases (*24, 38–40*), iron pipe scales should also be examined for the presence of vanadinite or other vanadium-rich phases. Accumulation via sorption is likely a readily reversible reaction, and could be more prone to release into the water with typical water chemistry or treatment changes (*15, 38–40*). If present, this could prove to be an even greater risk to consumers because most distribution systems contain large amounts of various types of iron pipes.

Further, because the vanadate ion essentially replaces the phosphate ion in the pyromorphite and hydroxyapatite structures in order to form vanadinite, the question arises as to the potential for water systems applying orthophosphate-based corrosion inhibitors to either destabilize vanadinite or inhibit its accumulation by preferential formation of pyromorphite family or other Pb(II) orthophosphate phases. Mobilization of vanadium from pipe scales could

conceivably provide an unexpected and unmonitored detrimental human exposure event.

Clearly, more research needs to be done to determine the presence, speciation, mineral associations, and concentration of vanadium in all types of drinking water distribution system pipes and deposits to better assess the chemical factors controlling the formation and release of vanadium and to understand and mitigate any potential public health threat. Further refinement of the solubility constant for vanadinite would also be very valuable to environmental and geoscience fields.

Acknowledgments

PNC/XOR facilities at the Advanced Photon Source, and research at these facilities, are supported by the U.S. Department of Energy−Basic Energy Sciences, a major facilities access grant from NSERC, the University of Washington, Simon Fraser University, and the Advanced Photon Source. Use of the Advanced Photon Source is also supported by the U.S. Department of Energy, Office of Science, Office of Basic Energy Sciences, under Contract DE-AC02-06CH11357. All ICP analyses were conducted by the United States Geological Survey's Mineral Resource Surveys Program under Interagency Agreement DWI4999901 under the direction of Dr. Stephen A. Wilson. We thank M. K. DeSantis (Pegasus Technical Services, Inc.) for scale photography, color descriptions, and scale harvesting of most of the specimens and Christina Bennett-Stamper for collecting the SEM-EDAX data. We are grateful for the helpful information and suggestions by Dr. Richard B. Wanty, U.S. Geological Survey, and for the pipe specimens provided by the numerous unnamed water system staffs and their consultants. We also thank Dr. Steve Heald for use of his computer programs in portions of the data processing and Dr. Robert Gordon for providing some standard material for the XANES analysis. Disclaimer: The U.S. Environmental Protection Agency through its Office of Research and Development funded and managed the research described here. It has not been subject to Agency review and, therefore, does not necessarily reflect the views of the Agency. Mention of trade names of commercial products and companies does not constitute endorsement or recommendation for use.

Note Added after ASAP Publication

There was an error in Figure 3 in the version of this paper published ASAP May 12, 2009; the corrected version published ASAP June 11, 2009.

Supporting Information Available

Details on analytical methodology, powder, and synchrotron XRD analysis, XANES LCF data, SEM-EDXA images, and thermodynamic calculations. This material is available free of charge via the Internet at http://pubs.acs.org.

Literature Cited

(1) Byczkowski, J. Z.; Kulkarni, A. P. Oxidative stress and pro-oxidant biological effects of vanadium, In *Vanadium in the Environment: Part Two Health Effects, Advances in Environmental Science and Technology*; John Wiley & Sons: New York 1998; p *403*.

(2) Stohs, S. J.; Bagchi, D. Oxidative mechanisms in the toxicity of metal ions. *Free Radical Biol. Med.* **1995**, *18* (2), 321–336.

(3) Panichev, N.; Mandiwana, K.; Moema, D.; Molatlhegi, R.; Ngobeni, P. Distribution of vanadium(V) species between soil and plants in the vicinity of vanadium mine. *J. Hazard. Mater.* **2006**, *A137*, 649–653.

(4) Crans, D. C.; Amin, S. S.; Keramidas, A. D. Chemistry of relevance to vanadium in the environment, In *Vanadium in the Environment*; John Wiley & Sons, Inc.: New York 1998; Vol*30*, pp 73−95.

(5) Minelli, L.; Veschetti, E.; Giammanco, S.; Mancini, G.; Ottaviani, M. Vanadium in Italian waters: monitoring and speciation of V(IV) and V(V). *Microchem. J.* **2000**, *67* (1−3), 83–90.

(6) Schock, M. R.; Kelty, K. C. Vanadium Chemistry Essentials for Treatment Studies. *Inorganics Contaminants Workshop (extended abstract)*, San Diego, CA, February 3−5, 2002.

(7) Veschetti, E.; Maresca, D.; Lucentini, L.; Ferretti, E.; Citti, G.; Ottaviani, M. Monitoring of V(IV) and V(V) in Etnean drinking-water distribution systems by solid phase extraction and electrothermal atomic absorption spectrometry. *Microchem. J.* **2007**, *85* (1), 80–87.

(8) Wehrli, B.; Stumm, W. Vanadyl in natural waters: Adsorption and hydrolysis promote oxidation. *Geochim. Cosmochim. Acta* **1989**, *53*, 69–77.

(9) Blackmore, D. P. T.; Ellis, J.; Riley, P. J. Treatment of a vanadium-containing effluent by adsorption/coprecipitation with iron oxyhydroxide. *Water Res.* **1996**, *30* (10), 2512–2516.

(10) Langmuir, D. *Aqueous Environmental Geochemistry*; Prentice-Hall: Upper Saddle River, NJ, 1997.

(11) Langmuir, D. Uranium solution-mineral equilibria at low temperatures with applications to sedimentary ore deposits. *Geochim. Cosmochim. Acta* **1978**, *42*, 547–569.

(12) Wanty, R. B.; Goldhaber, M. B. Thermodynamics and kinetics of reactions involving vanadium in natural systems: Accumulation of vanadium in sedimentary rocks. *Geochim. Cosmochim. Acta* **1992**, *56* (4), 1471–1483.

(13) Howd, R. A. Proposed Notification Level for Vanadium. http://oehha.ca.gov/water/pals/vanadium.html (accessed September 12, 2008).

(14) U. S. Environmental Protection Agency. Drinking water contaminant candidate list 3—Draft; Notice *Fed. Regist.* **2008**, *73: 35*, 9627−9654.

(15) Schock, M. R.; Hyland, R. N.; Welch, M. M. Occurrence of contaminant accumulation in lead pipe scales from domestic drinking-water distribution systems. *Environ. Sci. Technol.* **2008**, *42* (12), 4285–4291.

(16) Briggs, P. H. The determination of forty elements in geological and botanical samples by inductively coupled plasma-atomic emission spectrometry, Ch. G. In *Analytical methods for chemical analysis of geologic and other materials*; U.S. Geological Survey Open File Report 02−223; U.S. Geological Survey: Denver, CO, 2002.

(17) Schock, M. R. Understanding corrosion control strategies for lead. *J. Am. Water Works Assoc.* **1989**, *81* (7), 88–100.

(18) Schock, M. R.; Scheckel, K. G.; DeSantis, M.; Gerke, T. L. Mode of Occurrence, Treatment and Monitoring Significance of Tetravalent Lead. *Proceedings of the American Water Works Association Water Quality Technology Conference*, Quebec City, Canada, November 6−10, 2005.

(19) Schock, M. R.; Wagner, I.; Oliphant, R. The Corrosion and Solubility of Lead in Drinking Water. In *Internal Corrosion of Water Distribution Systems*, 2nd; AWWA Research Foundation/TZW: Denver, CO 1996; pp 131−230.

(20) Nriagu, J. O.; Pirrone, N. Emission of vanadium into the atmosphere. In *Vanadium in the Environment, Part 1, Advances in Environmental Science and Technology*; John Wiley & Sons Inc: New York 1998; Vol *30*, pp 25−36.

(21) Chaurand, P.; Rose, J.; Briois, V.; Salome, M.; Proux, O.; Nassif, V.; Olivi, L.; Susini, J.; Hazemann, J. L.; Bottero, J. Y. New Methodological approach for the vanadium K-edge X-ray absorption near-edge structure interpretation: application to the speciation of vanadium in oxide phases from steel slag. *J. Phys. Chem. B* **2007**, *111* (19), 5101–5110.

(22) Wong, J.; Lylte, F. W.; Messmer, R. P.; Maylotte, D. H. K-edge absorption spectra of selected vanadium compounds. *Phys. Rev. B* **1984**, *30* (10), 5596–5610.

(23) Anthony, J. W.; Bideaux, R. A.; Bladh, K. W.; Nicholas, M. C. *Handbook of Mineralogy Volume V Borates, Carbonate, Sulfates*; Mineral Data Publishing: Tucson, 2003; Vol. V.

(24) Anthony, J. W.; Bideaux, R. A.; Bladh, K. W.; Nicholas, M. C. *Handbook of Mineralogy Volume IV Arsenates, Phosphates, Vanadates*; Mineral Data Publishing: Tucson, AZ, 2000; Vol. IV.

(25) Zhang, P.; Ryan, J. A. Formation of pyromorphite in anglesite-hydroxyapatite suspensions under varying pH conditions. *Environ. Sci. Technol.* **1998**, *32* (21), 3318–3324.

(26) Zhang, P.; Ryan, J. A. Formation of chloropyromorphite from galena (PbS) in the presence of hydroxyapatite. *Environ. Sci. Technol.* **1999**, *33* (4), 618–624.

(27) Zhang, P.; Ryan, J. A. Transformation of Pb(II) from cerussite to chloropyromorphite in the presence of hydroxyapatite under varying conditions of pH, *Environ. Sci. Technol.* **1999**, *33* (4), 625–630.

(28) Zhang, P.; Ryan, J. A.; Bryndzia, L. T. Pyromorphite formation from goethite adsorbed lead. *Environ. Sci. Technol.* **1997**, *31*, 2673–2678.

(29) Schock, M. R.; Giani, R. Oxidant/Disinfectant Chemistry and Impacts on Lead Corrosion, Sunday Workshop American Water Works Association Water Quality Technology Conference, San Antonio, TX, November 14, 2004.
(30) Schock, M. R.; Lytle, D. A. New Insights into Lead and Copper Corrosion Control and Treatment Change Impacts. *Proceedings of the American Water Works Association Annual Conference and Exposition*, Toronto, ON, June 24−28, 2007.
(31) Garrels, R. M. Some free energy values from geologic relations. *Am. Mineral.* **1957**, *42*, 780–791.
(32) Schock, M. R. Causes of Temporal Variability of lead in domestic plumbing systems. *Environ. Monit. Assess.* **1990**, *15*, 59–82.
(33) James, C. N.; Copeland, R. C.; Lytle, D. A. Relationships between Oxidation-Reduction Potential, Oxidant, and pH in Drinking Water *Proceedings of the American Water Works Association Water Quality Technology Conference*, San Antonio, TX, November 14−18, 2004.
(34) Rajasekharan, V. V.; Clark, B. N.; Boonsalee, S.; Switzer, J. A. Electrochemistry of free chlorine and monochloramine and its relevance to the presence of Pb in drinking water. *Environ. Sci. Technol.* **2007**, *41* (12), 4252–4257.
(35) Bethke, C. M.; Yeakel, S. *The Geochemist's Workbench® Release 7.0 Reference Manual*; Rockware, Inc.: Golden, CO, 2007.
(36) *National Institute of Standards and Technology.* NIST Standard Reference Database 46: NIST Critically Selected Stability Constants of Metal Compexes Database, Version 6.0 for Windows; U.S. Department of Commerce: Gaithersburg, MD 2001.
(37) Brinza, L.; Benning, L. G.; Statham, P. J. Adsorption Studies of Mo and V onto ferrihydrite. *Mineralogical Magazine* **2008**, *72* (1), 385–388.
(38) Schock, M. R. Distribution systems as contamination reservoirs: Is a new paradigm needed for treatment and monitoring? *Inorganic Contaminants Workshop (extended abstract), Reno, NV, February 1−3*, 2004.
(39) Schock, M. R. Distribution Systems as Reservoirs and Reactors for Inorganic Contaminants, Ch. 6. In *Distribution System Water Quality Challenges in the 21st Century*; American Water Works Association: Denver, CO, 2005; pp 105−140.
(40) Schock, M. R. Unsolved problems with corrosion and distribution system inorganics. *AWWA 2007 Research Symposium*, Reno, NV, March 2−3, 2007.

ES900501T

Supporting Information For:

Identification and Distribution of Vanadinite ($Pb_5(V^{5+}O_4)_3Cl$) in Lead Pipe Corrosion By-products

Tammie L. Gerke [1], Kirk G. Scheckel[2], and Michael R. Schock[2*]

Twenty-two pages containing four appendices, three figures, and five tables:

* Corresponding author phone: 513-569-7412; fax 513-569-7172 email: Schock.Michael@epa.gov
[1] Department of Geology, University of Cincinnati, Cincinnati, OH 45221-0013
[2] USEPA, NRMRL, 26 West Martin Luther King Drive, Cincinnati, OH 45268

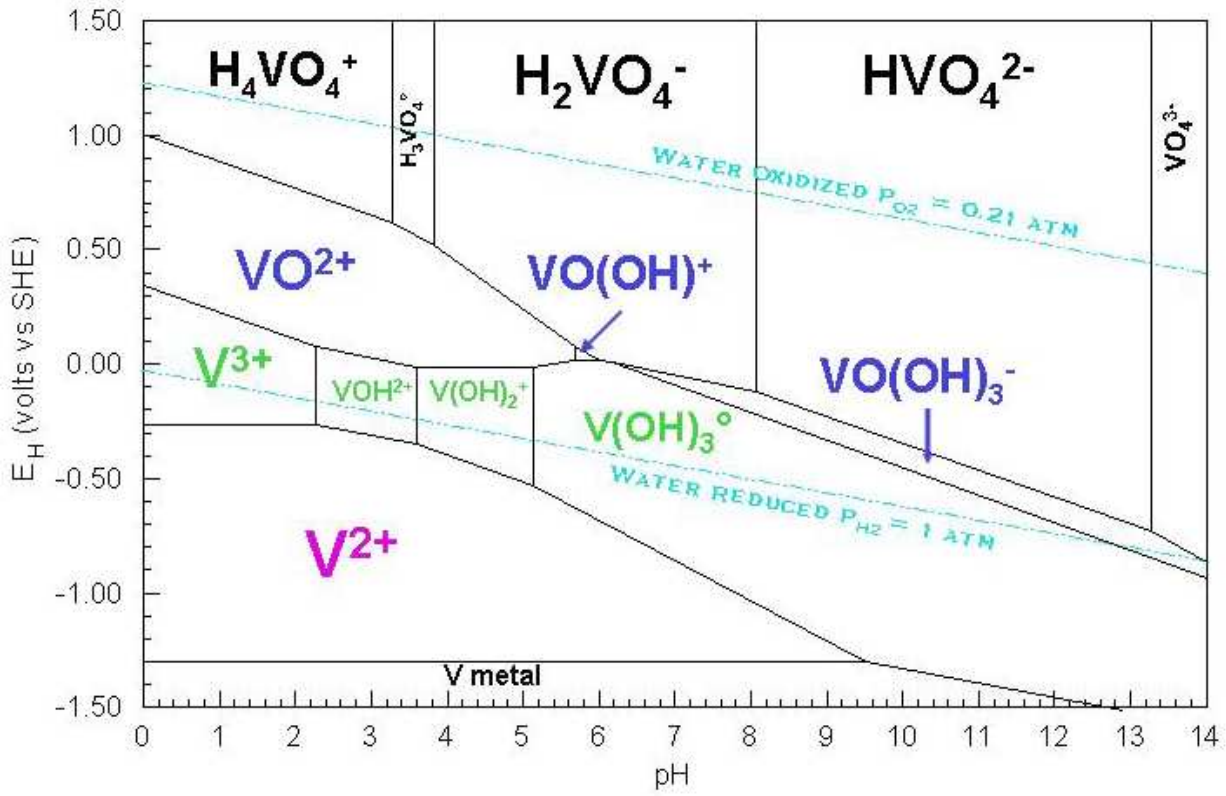

Figure SI1. Diagram of the predominant aqueous vanadium species assuming dissolved vanadium species activities of 0.1 mg/L at 25°C, and an ionic strength of zero.

Appendix A. Analytical Methodology

Traditional Powder XRD

All samples were analyzed using a Scintag XDS-2000 theta-theta diffractometer system equipped with a Peltier detector using a Cu Kα radiation at 40 kV and either 30 or 40 mA. The typical analysis used a 2θ range from 5° to 90 °, with a 0.02° step, and a 2 second count time at each step. Alternative conditions were used occasionally to clarify certain spectral features. Crystalline phase identifications were made using Jade XRD software (Version 8.0, MDI Incorporated, Livermore, CA) and the International Center for Diffraction Data 2002 PDF-2 release, in general accordance with ASTM Standard Practices *(1,2)*. Depending on the amount of sample available, the ground powders were either filled into a well in zero-background quartz

plates, or were evaporated in a slurry with AR-grade amyl acetate onto a flat zero-background quartz plate (Gem Dugout, State College, PA).

ICP-OES

Aliquots of samples were analyzed at the United Stated Geological Survey (USGS) facilities in Denver, Colorado in accordance with USGS procedures *(3)* using a Perkin Elmer/Sciex Elan 3000 spectrophotometer. The samples were analyzed for a wide spectrum of elements but only vanadium and lead concentrations are reported here (Table 1).

SEM

Secondary electron images and elemental maps were obtained using a JEOL 5800 Scanning Electron Microscope with an attached Link Analytical energy dispersive X-ray analyzer. The accelerating voltage was 20 keV and an average count time of three to five minutes was used to obtain all EDXA elemental maps. The magnification used ranged from approximately 100x to 500x and samples were carbon coated.

Synchrotron

Sample Preparations

Nineteen randomly selected lead corrosion by-product layers from 12 lead pipes representing seven of the eight distribution systems were processed for bulk XANES analysis (Table 1). A thin layer of prepared corrosion by-product material was smeared onto Kapton tape and folded back on itself.

All *in-situ* micro-X-ray fluorescence elemental maps (μ-XRF maps) corresponding micro-X-ray diffraction (μ-XRD) analyses, and XANES analyses were conducted using thin sections of three lead pipes with their corrosion by-products *in-situ* from two distribution systems (Table 1). These pipe samples were not the same as any of the samples utilized for the bulk XANES analysis. Thin sections were prepared by encasing segments of lead pipe in Buehler Epo Thin® Low Viscosity Epoxy, mounting them on quartz slides and polished to a thickness of approximately 35 microns. Each section was digitally photographed using a Canon G3 digital camera mounted to a copy stand.

Linear combination fitting refers to the process of selecting a multiple component fitting function (a Levenberg-Marquardt least-squares algorithm in this study) that minimizes the sum of the squares of residuals. During the fitting procedure, residual error (the normalized root square difference between the sample spectra and fitted data) was minimized by removal of non-essential reference components and continued until no net improvement of residual error was observed. The parameters of the theoretical function model are the desired physical descriptors of the measurements in which one attempts to fit the data to the model and report the parameter values (often as a weight or fractional percent of the total). The accuracy of the fitting procedure depends upon data quality and measured limits in addition to how well the reference standards actually represent the soil samples. We utilized a fit range of -10 to 70 eV for the XANES spectra which encompassed 289 data points and four variables. The best fitting scenarios, determined by the smallest residual error and the sum of all fractions being close to 1, are shown in Table SI2. A minimum of 2 components were necessary to fully describe any particular sample within 1% reproducible error indicating that two V species could be tested statistically

stringent. The fundamental source of fitting error is typically due to the limited number of actuators that afford a limited number of degrees of freedom for which, in our case, we restricted error significantly. The reference samples included in the principal component analysis and LCF fitting procedure included vanadinite, lenoblite, V(V) oxide, mixed V(IV,V) oxide, and V metal.

20-BM

Bulk XANES

V (5465 eV) K-XANES data were collected with electron storage ring operated at 7 GeV with a current of 101 mA. Three to five scans were collected at ambient temperature in fluorescence mode with a solid-state 13-element detector. A 0.5 mm pre-monochromator slit width and a Si(III) double crystal monochromator detuned by 10% to reject higher-order harmonics was employed. The beam energy was calibrated by assigning the first inflection of the absorption edge of vanadium metal foil to 5465 eV. Reference samples of various vanadium-rich phases were collected for comparison with the XANES spectra (Figure 1b; Table 2). The collected scans for a particular sample were averaged, the data were then normalized, and the background was removed by spline fitting using IFEFFIT *(4)*.

20-ID

micro-XRF

X-ray micro-beam studies (fluorescence and diffraction) were performed at XOR/PNC 20-ID of the Advanced Photon Source (APS), Argonne National Laboratory (Argonne, IL) under standard operating conditions (7 GeV and ring current of 101 mA in top-up mode). μ-XRF maps were recorded using a multi-element solid-state Ge energy dispersive detector (Canberra). The

monochromatic beam energy was set at 13.1 KeV using a Si (111) channel-cut monochromator and the beam was focused to approximately 15 x 15 μm using rhodium-coated Kirkpatrick-Baez focusing optics. μ-XRF maps were obtained using various step sizes and counts per pixel. Micro regions of interest within the lead scales were selected for additional analyses (μ-XRD and XANES) based on the elemental data obtained from μ-XRF maps.

micro-XRD

A MAR 165 charge-coupled detector (CCD) was used for microcrystallography (μ-XRD) studies and was positioned at approximately 190 mm from the sample. Two dimensional μ-XRD patterns were collected for 60 to 120 s at 15 KeV with a wavelength (λ) of 0.8265 Å. Two-dimensional diffractograms (2D Debye-Scherrer rings) were converted to one-dimensional 2θ scans using the software package Fit2D [5]

micro-XANES

V (5465 eV) K-XANES data were collected with electron storage ring operated at 7 GeV with a current of 101 mA. Three scans were collected at ambient temperature in fluorescence mode with a solid-state 13-element detector. A 0.5 mm pre-monochromator slit width and a Si(III) double crystal monochromator detuned by 10% to reject higher-order harmonics was employed. The beam energy was calibrated by assigning the first inflection of the absorption edge of vanadium metal foil to 5465 eV. Reference samples of various vanadium-rich phases were collected for comparison with the XANES spectra (Figure 1b; Table 2). The collected scans for a particular sample were averaged, the data were then normalized, and the background was removed by spline fitting using IFEFFIT *(4)*.

Table SI1. Most abundant crystalline lead phases identified by powder X-ray diffraction.

Sample ID	Layer	Cerussite $PbCO_3$	Hydrocerussite $Pb_3(CO_3)_2(OH)_2$	Plattnerite PbO_2	Litharge PbO	Pb^{II} orthophosphate(s) $Pb_5(PO_4)_3(OH,Cl,F)$, $Pb_9(PO_4)_6$
A1	L1			X		
	L2			X		
A2	L1			X		
	L2			X		
A3	L1			X		X
	L2			X		
	L3			X	X	
A4	L1			X		
	L2			X		
	L3			X		
	L4			X		
A5	L1			X		X
	L2		X			
	L3			X		
A6	L1					X
	L2			X		
	L3			X		
A7	L1			X		X
	L2					X
	L3				X	
B1	whole		X			
C1	L1					
	L2		X			
	L3		X			
D1	L1		X			
E1	L1	X				
	L2	X				
	L3	X				
F1	L1	X	X			
G1	L1			X		
H1	L1		X			
I1	L1	X				
	L2	X				
	L3	X				

Table SI2. Linear combination fitting results for XANES spectra in Figure 1. Data presented as weighted percents over a fit range of -10 to 70 eV.

	References					
Sample	**Vanadinite**	**Lenoblite**	**V(V) Oxide**	**V(IV,V) Oxide**	**V metal**	**R-factor [a]**
A5 L1	91.4		8.6			0.002
D1 L1	89.8		10.2			0.005
G1 L1	92.6		7.4			0.004
A6 PtB	95.2		4.8			0.002
I1 PtH	98.1		1.9			0.002

[a] R-factor = $[(\text{data-fit})^2]/[\text{data}^2]$

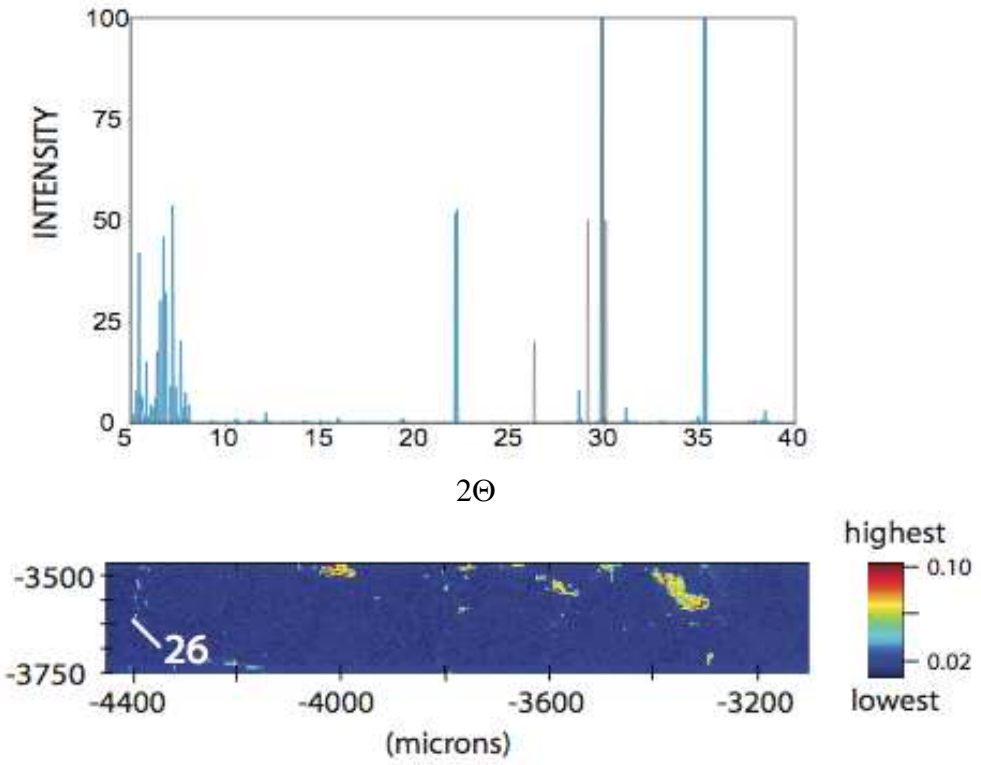

Figure SI2: Example μ-XRF map of vanadium concentrations for a selected region of sample A6. The numbered location in the μ-XRF maps indicates the location of the representative μ-XRD trace. The μ-XRD trace is in blue and the main XRD identification peaks for vanadinite are indicated by gray transparent lines between 25 and 31 2Θ. This example shows typically poor agreement between the reference XRD vanadinite peaks and the μ-XRD pattern.

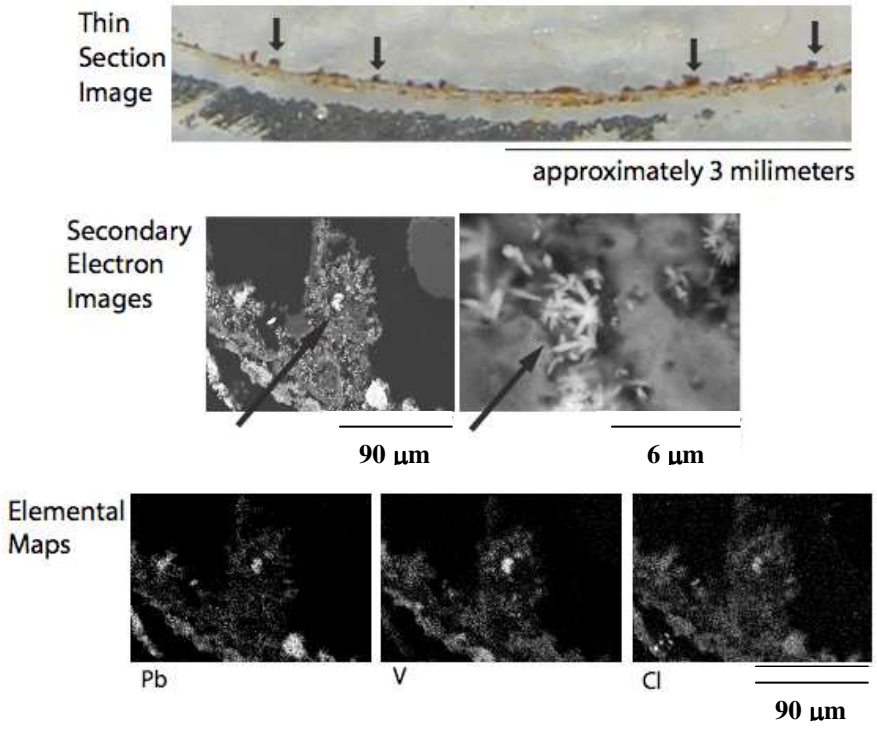

Figure SI3: Thin-section image for sample A6. Arrows indicate regions where grains of vanadinite were identified. One representative region was imaged with secondary electrons at two different scales (arrow points to vanadinite grains) and elemental maps for vanadium (V), lead (Pb), and chlorine (Cl) were obtained. Scales are provided for all images.

Appendix B: Example Calculations for derivation of approximate upper limit for log K_{sp} and $\Delta G_f°$ for vanadinite

Using the general background water chemistry and assumptions about the limits of the highly varying water matrix constituents (which would affect ionic strength and particularly lead speciation), a range of log K_{sp} and $\Delta G_f°$ values for presumed equilibrium with vanadinite can be calculated. The text discusses some important factors pertaining to the estimation of the dissolved lead(II) concentration in the water, and what assumptions were made here. In addition, there is a possibility that the dissolved lead(II) concentration was considerably over 200 micrograms per liter for prolonged periods of time at utility A, when reductive dissolution of the PbO_2 deposits were taking place. Two different logical paths can be taken with respect to this phenomenon, and they would result in different presumptions of total soluble lead for the modeling. On the one hand, there was a very high lead concentration during stagnation for several years, which could suggest that log K_{sp} for vanadinite would be much higher than is computed here. However, following the trend of analysis of V in the pipe deposits from this water system, indicates that the V concentrations in the scale appear to actually be increasing slightly with continued exposure to the phosphate treatment chemical, and when soluble lead release was lower, but background water redox conditions were stabilizing to lead(II)-orthophosphate precipitation and formation within the outer scale layers. Analyses of V-rich scales from other water systems for which reasonable estimates of redox and lead release conditions can be made with some confidence, further suggest that Pb concentrations need not be in the hundreds of micrograms per liter to form vanadinite. Thus, we have concluded that during the initial highly-plumbosolvent conditions of rampant reductive dissolution at this water

system, the scale removal rate physically constrained the ability of vanadinite to form and remain stable within the scale itself. Only further detailed lead speciation research in the laboratory and with future field investigations will really resolve this apparent paradox.

The computer program Geochemist's Workbench (Release 7, Rockware Inc., Golden, CO) was used to perform the speciation calculations *(6)*. The temperature was assumed to be 25°C, because there are few reliable temperature functions for adjusting the lead and vanadium equilibrium constants to other temperatures. Sodium was used to balance charge, as it would have minimal impact on the actual fraction of the metals complexed. Equilibrium constants for vanadium species were used as furnished in the "thermo.dat" data file, and generally followed Wanty and Goldhaber (1992) *(7)*. Equilibrium constants for lead species were taken from NIST (2001) for aqueous complexes or from Schock et al. (1996) *(8,9)*. The NIST formation constants for lead carbonate complexes are considerably smaller than those used for previous solubility computations by Schock et al. *(9)* and many references cited therein, which could be a source of bias in the estimation performed here. As noted, these computed values likely represent an approximate upper bound to the solubility of vanadinite, as during normal water usage and flow patterns in the premises, as well as with typical treatment and seasonal water variability, lead and vanadium concentrations are probably usually lower than the assumptions here. There is also some variability in the inorganic carbon concentration and pH over the year, so that adds more complication to handling all possible combinations of background constituent concentrations.

Table SI3. Water quality for utility A used to derive log K_{sp} for vanadinite.

Parameter	**City A**
pH	7.6
Total Alkalinity (mg/L as HCO_3)	74
E_h (est,volts vs SHE)	.700
mg/L (in units indicated)	
Aluminum	.08
Calcium	46
Chloride	16-89
Fluoride	1
Lead (μg/L)	7, 10, 15
Magnesium	9.9
Nitrate	13.3
Orthophosphate	2.3
Potassium	3
Silica	--
Sodium	16
Sulfate	54
Vanadium	.0009

Table SI4. Computation of limits to ΔG^{o}_{f} for vanadinite.

$K_{sp}=\{Pb^{2+}\}^{5}\{VO_4^{3-}\}^{3}\{Cl^{-}\}$ $\log K_{sp} = -[\Delta G^{\circ}_{r}/5.7077]$

$R=8.314E^{-3}$ kJ/mol×deg

	kJ/mol	
ΔG°_{f} Cl^{-}	**-131.23**	Wanty & Goldhaber 1992
ΔG°_{f} Pb^{2+}	**-24.69**	
ΔG°_{f} VO_4^{3-}	**-899.00**	Wanty & Goldhaber 1992

Input Total Concentrations			Computed Activities			Computed $\log K_{sp}$	Computed ΔG°_{r}	Computed ΔG°_{f} vanadinite
Cl^{-}	Pb^{2+}	V as VO_4^{3-}	Cl^{-}	Pb^{2+}	VO_4^{3-}			
City A Data								
89	0.007	0.002	-2.6456	-8.5072	-13.7804	-86.5228	493.8462	-3445.5
16	0.007	0.002	-3.3865	-8.5020	-13.7729	-87.2152	497.7982	-3449.5
89	0.010	0.002	-2.6468	-8.3493	-13.7804	-85.7345	489.3468	-3441.0
16	0.010	0.002	-3.3865	-8.3471	-13.7729	-86.4407	493.3776	-3445.1
89	0.015	0.002	-2.6468	-8.1732	-13.7804	-84.8540	484.3212	-3436.0
16	0.015	0.002	-3.3865	-8.1710	-13.7729	-85.5602	488.3520	-3440.0
Average:						-86.0546	491.1737	-3442.9

Table SI5. Example computation from Geochemist's Workbench for ion activity product of vanadinite assuming equilibrium, for case with Cl^- = 16 mg/L, V= 0.002 as VO_4^{3-} and Pb = 0.010 mg/L (Table SI4).

```
Temperature =  25.0 C     Pressure =  1.013 bars
pH =  7.600               log fO2 =   -5.370
Eh =   0.7000 volts       pe =  11.8333
Ionic strength      =     0.005065
Activity of water   =     0.999984
Solvent mass        =     1.000000 kg
Solution mass       =     1.000242 kg
Solution density    =     1.013    g/cm3
Chlorinity          =     0.000446 molal
Dissolved solids    =          242 mg/kg sol'n
Rock mass           =     0.000000 kg
Carbonate alkalinity=        74.00 mg/kg as CaCO3
```

No minerals in system.

Aqueous species	molality	mg/kg sol'n	act. coef.	log act.
HCO3-	0.001447	88.26	0.9277	-2.8722
Ca++	0.001037	41.54	0.7466	-3.1113
SO4--	0.0004802	46.12	0.7373	-3.4509
Cl-	0.0004438	15.73	0.9254	-3.3865
Mg++	0.0003770	9.160	0.7552	-3.5456
Na+	0.0002186	5.025	0.9270	-3.6932
NO3-	0.0002105	13.05	0.9254	-3.7103
CO2(aq)	7.832e-005	3.446	1.0000	-4.1062
K+	7.558e-005	2.954	0.9254	-4.1553
CaSO4	5.724e-005	7.790	1.0000	-4.2423
F-	5.058e-005	0.9607	0.9262	-4.3293
CaHCO3+	1.865e-005	1.885	0.9287	-4.7615
MgSO4	1.702e-005	2.048	1.0000	-4.7690
HPO4--	1.287e-005	1.235	0.7373	-5.0227
MgHCO3+	4.219e-006	0.3599	0.9270	-5.4077
H2PO4-	4.126e-006	0.4000	0.9270	-5.4174
CaHPO4	4.035e-006	0.5489	1.0000	-5.3942
CO3--	3.273e-006	0.1963	0.7397	-5.6161
CaCO3	3.080e-006	0.3082	1.0000	-5.5115
Al(OH)4-	2.825e-006	0.2683	0.9270	-5.5819
MgHPO4	2.195e-006	0.2640	1.0000	-5.6585
Sr++	2.100e-006	0.1839	0.7420	-5.8074
CaCl+	1.719e-006	0.1298	0.9270	-5.7978
CaNO3+	1.297e-006	0.1324	0.9270	-5.9200
MgF+	9.067e-007	0.03925	0.9270	-6.0755
MgCO3	5.696e-007	0.04802	1.0000	-6.2444
CaF+	4.926e-007	0.02910	0.9270	-6.3404
CaPO4-	4.456e-007	0.06017	0.9270	-6.3840
OH-	4.431e-007	0.007534	0.9262	-6.3868
NaSO4-	3.825e-007	0.04552	0.9270	-6.4503
NaHCO3	3.661e-007	0.03075	1.0000	-6.4364
KSO4-	1.902e-007	0.02570	0.9270	-6.7537
MgCl+	1.783e-007	0.01065	0.9270	-6.7818
MgPO4-	1.639e-007	0.01954	0.9270	-6.8184

SrSO4	1.099e-007	0.02018	1.0000	-6.9589
Al(OH)3	6.428e-008	0.005013	1.0000	-7.1919
MgH2PO4+	3.711e-008	0.004500	0.9270	-7.4635
SrHCO3+	3.404e-008	0.005058	0.9270	-7.5010
PbCO3(aq)	3.387e-008	0.009047	1.0000	-7.4702
NaHPO4-	2.931e-008	0.003486	0.9270	-7.5659
H+	2.690e-008	2.710e-005	0.9338	-7.6000
MgOH+	1.979e-008	0.0008175	0.9270	-7.7364
VO2(OH)2-	1.504e-008	0.001759	0.9270	-7.8556
KHPO4-	7.853e-009	0.001060	0.9270	-8.1379
CaOH+	6.806e-009	0.0003885	0.9270	-8.2000
Pb++	6.080e-009	0.001259	0.7397	-8.3471
SrHPO4	5.492e-009	0.001008	1.0000	-8.2603
O2(aq)	5.378e-009	0.0001721	1.0013	-8.2688
PbOH+	4.851e-009	0.001087	0.9270	-8.3471
SrCO3	2.420e-009	0.0003572	1.0000	-8.6162
VO3OH--	2.139e-009	0.0002479	0.7373	-8.8022
NaCl	2.094e-009	0.0001223	1.0000	-8.6791
SrNO3+	2.065e-009	0.0003089	0.9270	-8.7181
Al(OH)2+	2.015e-009	0.0001229	0.9270	-8.7287
HF	1.738e-009	3.476e-005	1.0000	-8.7599
NaCO3-	1.690e-009	0.0001403	0.9270	-8.8050
PbHCO3+	1.530e-009	0.0004103	0.9270	-8.8482
NaF	1.253e-009	5.258e-005	1.0000	-8.9022
HSO4-	9.441e-010	9.162e-005	0.9270	-9.0579
PbSO4 (aq)	7.799e-010	0.0002364	1.0000	-9.1080
Mg2CO3++	7.620e-010	8.275e-005	0.7420	-9.2476
KCl	7.424e-010	5.534e-005	1.0000	-9.1293
SrF+	4.426e-010	4.717e-005	0.9270	-9.3870
PO4---	3.684e-010	3.498e-005	0.5034	-9.7317
Pb(CO3)2--	3.319e-010	0.0001086	0.7373	-9.6114
N2(aq)	2.051e-010	5.745e-006	1.0000	-9.6880
AlF2+	1.405e-010	9.128e-006	0.9270	-9.8852
SrPO4-	9.848e-011	1.798e-005	0.9270	-10.0396
PbCl+	7.932e-011	1.924e-005	0.9270	-10.1336
AlF3	7.660e-011	6.431e-006	1.0000	-10.1158
Pb(OH)2(aq)	5.793e-011	1.397e-005	1.0000	-10.2371
PbHPO4	5.370e-011	1.628e-005	1.0000	-10.2700
NaOH	5.220e-011	2.087e-006	1.0000	-10.2823
SrH2PO4+	3.613e-011	6.668e-006	0.9270	-10.4751
PbF+	2.794e-011	6.319e-006	0.9270	-10.5867
H3PO4	1.349e-011	1.322e-006	1.0000	-10.8698
AlHPO4+	9.638e-012	1.185e-006	0.9270	-11.0489
AlF++	9.427e-012	4.333e-007	0.7420	-11.1552
AlOH++	9.330e-012	4.103e-007	0.7420	-11.1597
KOH	9.110e-012	5.110e-007	1.0000	-11.0405
SrOH+	3.539e-012	3.702e-007	0.9270	-11.4840
VO(OH)3	3.519e-012	4.151e-007	1.0000	-11.4535
Pb(SO4)2--	2.257e-012	9.009e-007	0.7373	-11.7789
PbPO4-	2.255e-012	6.812e-007	0.9270	-11.6798
AlF4-	9.720e-013	1.001e-007	0.9270	-12.0453
PbH2PO4+	5.861e-013	1.783e-007	0.9270	-12.2649
HF2-	2.777e-013	1.083e-008	0.9270	-12.5894
Mg2OH+++	2.619e-013	1.718e-008	0.5314	-12.8565
PbCl2(aq)	4.571e-014	1.271e-008	1.0000	-13.3400
VO4---	3.351e-014	3.850e-009	0.5034	-13.7729
PbF2	2.977e-014	7.298e-009	1.0000	-13.5262

Al+++	2.780e-014	7.500e-010	0.5379	-13.8252
Pb(OH)3-	2.488e-014	6.423e-009	0.9270	-13.6371
AlSO4+	5.840e-015	7.184e-010	0.9270	-14.2665
AlF5--	4.242e-015	5.173e-010	0.7373	-14.5048
NO2-	1.395e-015	6.415e-011	0.9254	-14.8891
Pb2OH+++	6.789e-016	2.928e-010	0.4721	-15.4942
VO2HPO4-	6.719e-016	1.202e-010	0.9270	-15.2057
VO2+	1.902e-016	1.578e-011	0.9270	-15.7536
Al(SO4)2-	1.617e-016	3.543e-011	0.9270	-15.8241
AlH2PO4++	1.537e-016	1.905e-011	0.7420	-15.9428
VO2F	2.711e-017	2.763e-012	1.0000	-16.5668
PbCl3-	1.609e-017	5.042e-012	0.9270	-16.8265
HCl	8.195e-018	2.987e-013	1.0000	-17.0865
H2F2	8.096e-018	3.238e-013	1.0000	-17.0918
VO2(HPO4)2---	5.109e-018	1.404e-012	0.5034	-17.5897
Pb(OH)4--	3.057e-018	8.411e-013	0.7373	-17.6471
VO2SO4-	1.661e-018	2.972e-013	0.9270	-17.8126
VO2F2-	2.595e-019	3.138e-014	0.9270	-18.6188
AlF6---	1.564e-019	2.204e-014	0.5034	-19.1038
Pb3(OH)4++	5.936e-020	4.092e-014	0.7166	-19.3713
HNO2	5.390e-020	2.533e-015	1.0000	-19.2684
VO2H2PO4	2.763e-020	4.971e-015	1.0000	-19.5586
H2SO4	2.172e-020	2.130e-015	1.0000	-19.6631
Al2(OH)2++++	2.170e-020	1.908e-015	0.3459	-20.1247
PbCl4--	4.163e-021	1.452e-015	0.7373	-20.5130
VO2F3--	3.173e-022	4.439e-017	0.7373	-21.6309
Mg4(OH)4++++	1.068e-023	1.764e-018	0.3459	-23.4326
VOOH+	1.253e-024	1.052e-019	0.9270	-23.9348
Pb4(OH)4++++	1.121e-024	1.005e-018	0.2632	-24.5298
Al3(OH)4(5+)	6.075e-025	9.048e-020	0.1903	-24.9370
H4P2O7	4.493e-026	7.994e-021	1.0000	-25.3475
VO++	1.842e-026	1.232e-021	0.7420	-25.8644
VOF+	4.451e-027	3.825e-022	0.9270	-26.3844
VOSO4	1.450e-027	2.364e-022	1.0000	-26.8385
VOF2	6.837e-029	7.172e-024	1.0000	-28.1652
(VO)2(OH)5-	3.843e-031	8.411e-026	0.9270	-30.4483
VOF3-	1.252e-031	1.551e-026	0.9270	-30.9354
Pb6(OH)8++++	4.478e-033	6.175e-027	0.3065	-32.8625
Al13O4(OH)24(7+)	1.505e-034	1.238e-028	0.0387	-35.2348
VOF4--	2.391e-035	3.417e-030	0.7373	-34.7538
ClO4-	2.503e-036	2.489e-031	0.9262	-35.6348
V(OH)2+	4.619e-039	3.923e-034	0.9270	-38.3684
Pb++++	4.487e-042	9.294e-037	0.3065	-41.8617
VOH++	2.441e-042	1.658e-037	0.7420	-41.7420
H2(aq)	1.049e-042	2.115e-039	1.0013	-41.9785
(VO)2(OH)2++	8.495e-044	1.426e-038	0.7420	-43.2004
V+++	1.518e-047	7.733e-043	0.5034	-47.1167
VSO4+	1.452e-048	2.134e-043	0.9270	-47.8710
NH4+	5.354e-056	9.656e-052	0.9246	-55.3053
NH3	1.041e-057	1.772e-053	1.0000	-56.9827
NH4SO4-	1.646e-058	1.877e-053	0.9270	-57.8166
V2(OH)2++++	4.259e-083	5.787e-078	0.3459	-82.8317
HS-	1.499e-133	4.954e-129	0.9262	-132.8576
H2S(aq)	3.107e-134	1.059e-129	1.0000	-133.5076
CH4(aq)	9.054e-139	1.452e-134	1.0013	-138.0426
S--	9.306e-140	2.983e-135	0.7420	-139.1608
CH3COO-	3.000e-144	1.771e-139	0.9277	-143.5554

MgCH3COO+	1.593e-146	1.327e-141	0.9270	-145.8308
HCH3COO	3.989e-147	2.395e-142	1.0000	-146.3991
NaCH3COO	3.705e-148	3.039e-143	1.0000	-147.4312
CaCH3COO+	1.530e-148	1.516e-143	0.9270	-147.8483
SrCH3COO+	6.433e-149	9.432e-144	0.9270	-148.2245
AlCH3COO++	4.079e-155	3.508e-150	0.7420	-154.5190
S2--	2.970e-238	1.904e-233	0.7373	-237.6595
S4--	0.0000	0.0000	0.7373	-300.0000
S3--	0.0000	0.0000	0.7373	-300.0000
Ca(O-phth)	0.0000	0.0000	1.0000	-300.0000
Al(O-phth)+	0.0000	0.0000	0.9270	-300.0000
H2(O-phth)	0.0000	0.0000	1.0000	-300.0000
Na(O-phth)-	0.0000	0.0000	0.9270	-300.0000
H(O-phth)-	0.0000	0.0000	0.9270	-300.0000
S6--	0.0000	0.0000	0.7373	-300.0000
S5--	0.0000	0.0000	0.7373	-300.0000
Al(O-phth)2-	0.0000	0.0000	0.9270	-300.0000
(O-phth)--	0.0000	0.0000	0.7373	-300.0000

Mineral saturation states

	log Q/K		log Q/K
Fluorapatite	21.2905s/sat	Arcanite	-10.0726
Hydroxyapatite	11.2984s/sat	MHSH(Mg1.5)	-10.3354
Chloropyromorphi	6.0019s/sat	Portlandite	-10.4887
Pyromorphite-Cl	5.9999s/sat	Ca(OH)2(c)	-10.4887
Whitlockite	5.7210s/sat	Thenardite	-10.6014
Vanadinite	2.5594s/sat	MgSO4(c)	-12.0182
Plumbogummite	1.4644s/sat	Gaylussite	-12.2707
Gibbsite	1.0145s/sat	Pirssonite	-12.4334
Dolomite	0.2780s/sat	Sr(NO3)2^4H2O	-13.2457
Dolomite-ord	0.2780s/sat	SrCl2^6H2O	-13.2519
Diaspore	0.2231s/sat	KNaCO3^6H2O	-13.4433
Strontianite	0.0037s/sat	Sr(NO3)2(c)	-13.5726
Calcite	-0.0965	Mg2Cl(OH)3^4H2O	-13.7867
Pyromorphite-OH	-0.1383	Mercallite	-13.8311
Pb3(PO4)2(c)	-0.2207	Antarcticite	-13.9971
Aragonite	-0.2614	Kainite	-14.4305
Cerussite	-0.4336	Plumbonacrite	-14.5738
Pb9(PO4)6	-0.6202	Plumbonacrite	-14.5738
Boehmite	-0.6213	CaCl2^4H2O	-14.7763
Hydroxypyromorph	-0.6516	Bischofite	-14.8477
Fluorite	-0.8111	V2O5(c)	-14.8530
Pb4O(PO4)2(c)	-0.8560	Hinsdalite	-14.9410
Pb3(PO4)2	-1.0467	SrCl2^2H2O	-15.1033
Monohydrocalcite	-1.0904	Hydromagnesite	-15.1771
Magnesite	-1.2543	MgOHCl	-15.3795
Dolomite-dis	-1.2664	Bloedite	-15.5706
CaHPO4^2H2O	-1.5768	MgV2O6(c)	-15.8471
PbHPO4(c)	-1.9411	SrCl2^H2O	-16.5796
Gypsum	-2.1189	K2CO3^3/2H2O	-17.0557
Hydrocerussite	-2.2333	Sr(OH)2(c)	-17.1649
Hydrocer (aged)	-2.2536	MgCl2^4H2O	-17.7760
Dawsonite	-2.2693	CaCl2^2H2O	-17.9805
Hydrocer (aged)	-2.2836	CaCl2^H2O	-18.1153
Anhydrite	-2.2970	Ca3V2O8(c)	-18.6834
Celestite	-2.8271	SrCl2(c)	-19.7417

Bassanite	-2.9259	Lime	-20.6053
Pb3(CO3)2(OH)2	-3.0436	Hydrophilite	-21.7030
CaSO4^1/2H2O(bet	-3.0945	Carnallite	-22.3184
Corundum	-3.4342	MgCl2^2H2O	-23.2133
Plattnerite	-3.4956	Ca2Cl2(OH)2^H2O	-24.1339
SrHPO4(c)	-3.8302	Na3H(SO4)2	-24.7899
Plattnerite	-3.8416	MgCl2^H2O	-26.5659
Nesquehonite	-3.9530	V2O4(c)	-29.8989
Anglesite	-3.9842	SrO(c)	-31.7271
MgF2(c)	-4.0257	KMgCl3^2H2O	-32.0032
Hydrocer(fresh)	-4.3036	Chloromagnesite	-32.3228
Berlinite	-4.3718	Burkeite	-33.9868
Brucite	-4.7845	KMgCl3	-39.3094
Epsomite	-5.1840	Al2(SO4)3^6H2O	-40.2659
Hexahydrite	-5.4207	Ca4Cl2(OH)6^13H2	-42.0248
Huntite	-5.5920	Tachyhydrite	-47.9659
Pentahydrite	-5.7615	Al2(SO4)3	-57.7270
SrF2(c)	-5.9276	V2O3(c)	-58.5712
Leonhardtite	-6.1500	PbF2(c)	-58.9134
Kieserite	-6.8867	K8H4(CO3)6^3H2O	-63.3675
Artinite	-7.0985	Graphite	-70.0192
Kalicinite	-7.3594	V3O5(c)	-72.7217
Alunite	-7.5942	V4O7(c)	-88.7502
Sylvite	-8.5012	Misenite	-92.4178
Halite	-8.6725	Sulfur-Rhmb	-99.4816
Spinel	-8.7887	Galena	-118.7591
Pb2Cl2CO3	-9.1213	(VO)3(PO4)2(c)	-121.2701
Ca2V2O7(c)	-9.3609	V	-125.0586
Mirabilite	-9.7461	SrS(c)	-148.3854
CaV2O6(c)	-9.7724	O-phth acid(c)	-554.7864

Gases	fugacity	log fug.
Steam	0.03131	-1.504
CO2(g)	0.002219	-2.654
O2(g)	4.268e-006	-5.370
N2(g)	3.139e-007	-6.503
H2(g)	1.360e-039	-38.867
H2S(g)	3.323e-133	-132.479
CH4(g)	5.993e-136	-135.222
S2(g)	1.381e-213	-212.860

		In fluid		Sorbed		Kd
Original basis	total moles	moles	mg/kg	moles	mg/kg	L/kg

Al+++	2.89e-006	2.89e-006	0.0780			
Ca++	0.00112	0.00112	45.0			
Cl-	0.000446	0.000446	15.8			
F-	5.20e-005	5.20e-005	0.987			
H+	6.29e-005	6.29e-005	0.0634			
H2O	55.5	55.5	1.00e+006			
HCO3-	0.00156	0.00156	94.9			
HPO4--	2.39e-005	2.39e-005	2.29			
K+	7.58e-005	7.58e-005	2.96			
Mg++	0.000402	0.000402	9.77			
NO3-	0.000212	0.000212	13.1			

Na+	0.000219	0.000219	5.04
O2(aq)	1.35e-008	1.35e-008	0.000431
Pb++	4.77e-008	4.77e-008	0.00987
SO4--	0.000555	0.000555	53.3
Sr++	2.25e-006	2.25e-006	0.197
V+++	1.72e-008	1.72e-008	0.000875

Elemental composition	In fluid		Sorbed	
	total moles	moles	mg/kg	moles	mg/kg

Aluminum	2.892e-006	2.892e-006	0.07800		
Calcium	0.001124	0.001124	45.02		
Carbon	0.001555	0.001555	18.68		
Chlorine	0.0004457	0.0004457	15.80		
Fluorine	5.198e-005	5.198e-005	0.9873		
Hydrogen	111.0	111.0	1.119e+005		
Lead	4.766e-008	4.766e-008	0.009873		
Magnesium	0.0004023	0.0004023	9.775		
Nitrogen	0.0002118	0.0002118	2.966		
Oxygen	55.52	55.52	8.880e+005		
Phosphorus	2.392e-005	2.392e-005	0.7406		
Potassium	7.578e-005	7.578e-005	2.962		
Sodium	0.0002194	0.0002194	5.043		
Strontium	2.254e-006	2.254e-006	0.1975		
Sulfur	0.0005552	0.0005552	17.79		
Vanadium	1.718e-008	1.718e-008	0.0008752		

References

(1) ASTM. **2003**. Standard Practices for Sampling Water-Formed Deposits. Volume 11.02, D 887-82. American Society for Testing and Materials, Conshohocken, PA.

(2) ASTM. **2003**. Standard Practices for Identification of Crystalline Compounds in Water-Formed Deposits by X-Ray Diffraction. Volume 11.02, D 934-80. American Society for Testing and Materials, Conshohocken, PA.

(3) Lamothe, P. J.; Meier, A. L.; Wilson, S. A. The determination of forty elements in aqueous samples by inductively coupled plasma-mass spectrometry, Ch. H In *Analytical methods for chemical analysis of geologic and other materials, U.S. Geological Survey*, Open File Report 02-223; U.S. Geological Survey: Denver, CO, 2002.

(4) Ravel, B.; Newville, M. ATHENA, ARTEMIS, HEPHAESTUS: data analysis for X-ray absorption spectroscopy using IFEFFIT. , *J. Synchrotron Rad.* **2005**, *12*, 537-541.

(5) Hammersley, A., *ESRF* **2001**, *10* (132).

(6) Bethke, C. M.; Yeakel, S. *The Geochemist's Workbench® Release 7.0 Reference Manual*; Rockware, Inc.: Golden, CO, 2007.

(7) Wanty, R. B.; Goldhaber, M. B. Thermodynamics and kinetics of reactions involving vanadium in natural systems: Accumulation of vanadium in sedimentary rocks, *Geochim. Cosmochim. Acta* **1992**, *56* (4), 1471-1483.

(8) National Institute of Standards and Technology *NIST Standard Reference Database 46: NIST Critically Selected Stability Constants of Metal Compexes Database, Version 6.0 for Windows*; U.S. Department of Commerce: Gaithersburg, MD, 2001.

(9) Schock, M. R.; Wagner, I.; Oliphant, R. The Corrosion and Solubility of Lead in Drinking Water, In *Internal Corrosion of Water Distribution Systems*; Second ed.; AWWA Research Foundation/TZW: Denver, CO, 1996; pp 131-230.